A Low-Profile Wide-Scan Magneto-Electric Dipole Antenna for 5G mm-Wave Communications

Maximilian Döring*, Nico Kästle, Thomas Frey, Felix Matt, Christian Waldschmidt, Tobias Chaloun
*University Ulm, Institute of Microwave Engineering, 89081 Ulm, Germany
Email: maximilian.doering@uni-ulm.de

***Abstract*—A low-profile magneto-electric dipole antenna for 5G communication networks is presented. The novel unit cell design exhibits a low complexity, facilitating a straightforward fabrication process. The antenna design operates from 24.25 GHz to 29.5 GHz, covering multiple frequency bands in the 5G New Radio Frequency Range 2. Across the operating band, a scan volume of up to 60° in the E- and 30° in the H-plane is achieved. The unit cell design was initially subjected to an infinite array analysis for optimization, followed by the fabrication of an 11 × 11 prototype antenna to validate the simulation results. The measured impedance bandwidth and the antenna gain are in good agreement with the simulations. The scan capability of the proposed magneto-electric dipole is validated through embedded element pattern measurements at 24.25 GHz, 27 GHz, and 29.5 GHz.**

***Index Terms*—phased array, planar antenna, wide-scan, magneto-electric dipole, mm-Wave, 5G.**

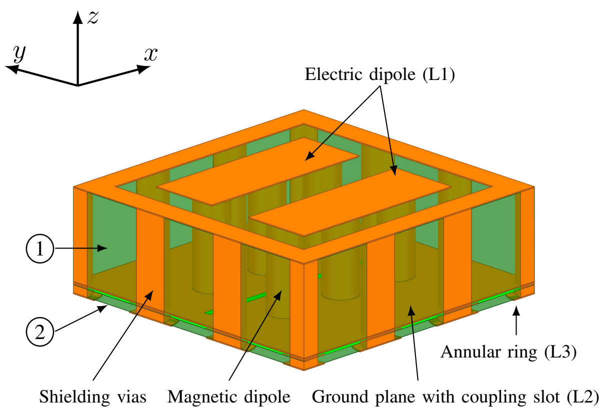

Fig. 1: Unit cell design of the magneto-electric dipole antenna.

I. Introduction

Presently, the focus of mobile communication networks is increasingly shifting towards utilizing the millimeter-wave (mm-wave) frequency bands. Within this context, the 5G New Radio Frequency Range 2 (FR2) protrude as an especially promising band for advancing the capabilities of 5G networks. FR2 exhibits distinctive advantages, characterized by its innate capacity to facilitate high data rates, minimize latency, and significantly enhance network capacity.

In order to reduce the costs and the hardware complexity, wideband antenna designs have gained popularity as they can efficiently cover multiple frequency bands. For instance, connected antenna arrays demonstrate such a wideband characteristic [1], although they tend to perform more efficiently for a larger aperture size. However, given the typically reduced strict specifications prevalent in mobile communication applications, smaller apertures often suffice. The magneto-electric (ME) dipole fully meets these requirements, making this type of antenna particularly well suited for small aperture sizes [2]. Moreover, the ME dipole can be fully realized in standardized printed circuit board (PCB) technology, allowing a straightforward low-cost manufacturing process [3]–[5].

In this contribution, a low-profile ME dipole antenna featuring wide-scan capabilities is introduced. The antenna design is implemented using standardized multilayer PCB technology. First, the unit cell (UC) design is discussed, subsequently conducting the infinite array analysis of the proposed ME dipole. In order to validate the simulation results an 11 × 11 prototype antenna is realized, showing good agreement with the simulation results. The excellent scan performance is demonstrated through embedded element pattern measurements.

II. Unit Cell Design

In the following section the UC design of the linear polarized ME dipole antenna is presented, as depicted in Fig. 1. The square-shaped UC dimension is $l_{\mathrm{UC}} = 5\,\mathrm{mm}$, preventing the onset of grating lobes in the operational frequency range from $24.25\,\mathrm{GHz}$ to $29.5\,\mathrm{GHz}$ up to a scan angle of $\vartheta = \pm 60°$. The antenna consists of two dielectric substrates, which are bonded together with the bonding film Rogers RO3001 ($\epsilon_{\mathrm{r}} = 2.28$). Thus, this PCB stackup allows a simple and standardized manufacturing process.

A bottom side microstrip line (MSL) feeding (L3) with a characteristic impedance of $50\,\Omega$ and an open-ended stub is employed, as depicted in Fig. 2b. The MSL feed excites the coupling aperture in the ground layer (L2). For better coupling and impedance matching, the MSL is tapered towards the open-ended stub, shown in Fig. 2b. The coupling aperture is realized through a resonant slot, exciting the ME dipole in the proposed design. However, this resonant slot aperture results in an increased front-to-back ratio [6]. In order to reduce spurious radiation from the feeding, a high permittivity substrate ② (in Fig. 1), namely Rogers RO3006 ($\epsilon_{\mathrm{r}} = 6.15$) with a height of $0.127\,\mathrm{mm}$ is used [7]. The upper dielectric substrate ① (in Fig. 1) consists of Rogers RO4003 ($\epsilon_{\mathrm{r}} = 3.55$) with a height of $1.524\,\mathrm{mm}$. The vias through substrate ① connect the ground plane with both metal patches (L1), shown in Fig. 1. These vias

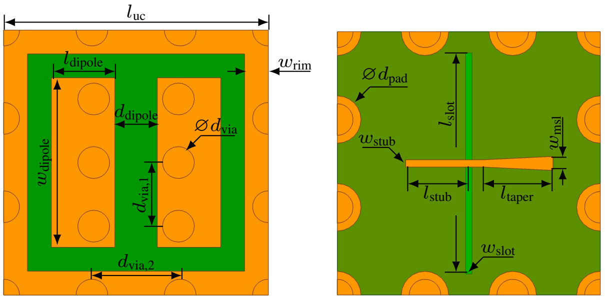

(a) (b)

Fig. 2: Parameterized a) top and b) bottom view of the proposed magneto-electric dipole UC design.

TABLE I: Design parameters of the magneto-electric dipole.

l_{uc}	5.00 mm	l_{dipole}	1.20 mm	w_{dipole}	3.20 mm
d_{dipole}	0.80 mm	w_{rim}	0.45 mm	d_{via}	0.60 mm
$d_{via,1}$	1.20 mm	$d_{via,2}$	1.33 mm	d_{pad}	0.90 mm
w_{msl}	0.26 mm	l_{taper}	1.20 mm	l_{stub}	1.20 mm
w_{stub}	0.14 mm	l_{slot}	4.20 mm	w_{slot}	0.12 mm

represent the magnetic dipole, since they create a quarter-wave shorted patch antenna. The metal patches on the top layer (L1) correspond to a conventional half-wavelength dipole realizing an electric dipole. By positioning the magnetic and electric dipole in perpendicular planes, they create the ME dipole. For the purpose of subsequent discussion, the E-plane within the proposed antenna design is defined along the y-z-axis and the H-plane along the x-z-axis, respectively. In order to reduce coupling to adjacent UCs and to suppress surface wave modes, shielding vias through both substrates surrounding the UC are implemented. The design parameters of the presented ME dipole are shown in Fig. 2 and the dimensions are listed in Tab. I.

III. Infinite Array Simulation

The proposed UC design was analyzed and optimized in an infinite array environment using the full wave simulation tool HFSS [8]. The investigation of the infinite array analysis spans a frequency range from 20 GHz to 35 GHz for scanning angles up to $\vartheta = 60°$. However, the intended operational frequency band is from 24.25 GHz to 29.5 GHz covering the 5G mm-wave bands n257, n258, and n261.

The simulated active reflection coefficients both in the E- and H-plane are illustrated in Fig. 3. In the E-plane the active reflection coefficient constantly remains below -10 dB within the operational frequency range for scanning angles up to 60°, as shown in Fig. 3a. In the H-plane the simulated active reflection coefficient exhibits an increase for larger scanning angles. Consequently, a scan volume up to 30° is achieved in the frequency range of 24.25 GHz to 29.5 GHz, while the active reflection coefficient remains below -10 dB (see Fig. 3b). Extending the scan volume up to $\vartheta = 60°$, the simulated active reflection coefficient within the H-plane remains below -5 dB in the operational frequency band.

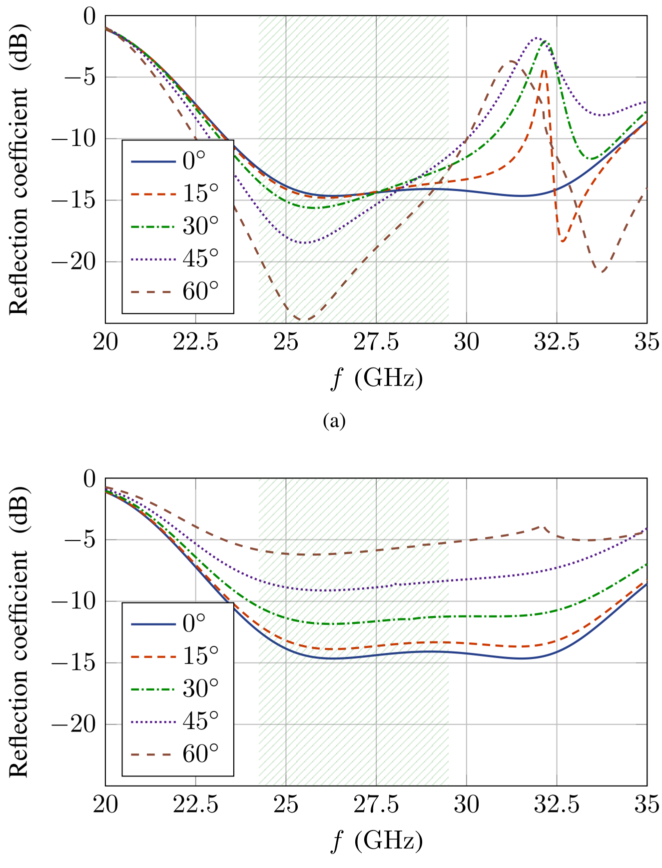

(a)

(b)

Fig. 3: Simulated active reflection coefficients in the (a) E- and (b) H-plane.

Considering the radiation efficiency, the active transmission coefficients from the feed to the corresponding Floquet mode can be used as a precise evaluation criterion [9]. The simulated active transmission coefficients in the co-polarization for both the E- and H-plane are depicted in Fig. 4. In the E-plane, the active transmission coefficient is defined by the fundamental TM(0,0) mode, and is presented in Fig. 4a for a scan range of up to 60°. The simulated active transmission coefficient for the E-plane remains above -1.28 dB in the operational frequency range from 24.25 GHz to 29.5 GHz. Regarding the scan performance in the H-plane, the simulated active transmission coefficient in the fundamental TE(0,0) mode consistently stays above -1.77 dB across the entire scanning range, as depicted in Fig. 4b. This slightly lower active transmission coefficient coincides with the simulated active reflection coefficients. The proposed ME dipole antenna demonstrates excellent polarization purity with a cross-polarization level below -40 dB for the E-plane and -35 dB for the H-plane.

IV. Realization and Measurement

An 11×11 prototype antenna has been manufactured and characterized, verifying the results obtained by the infinite array analysis, as shown in Fig. 5. Since only a passive

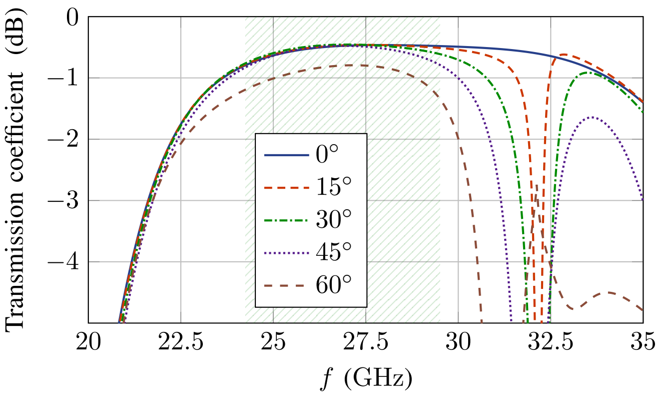

(a)

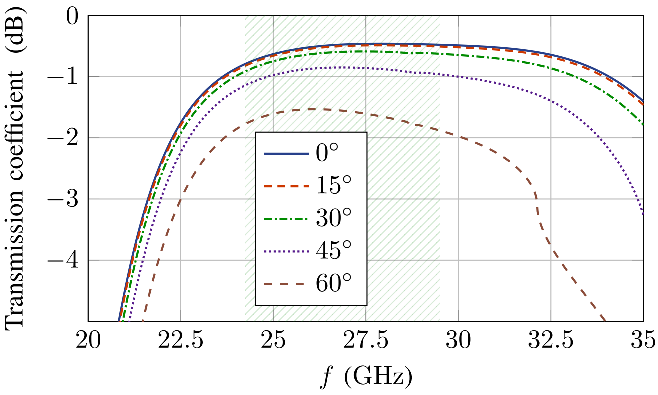

(b)

Fig. 4: Simulated active transmission coefficients in the co-polarization for the (a) E- and (b) H-plane.

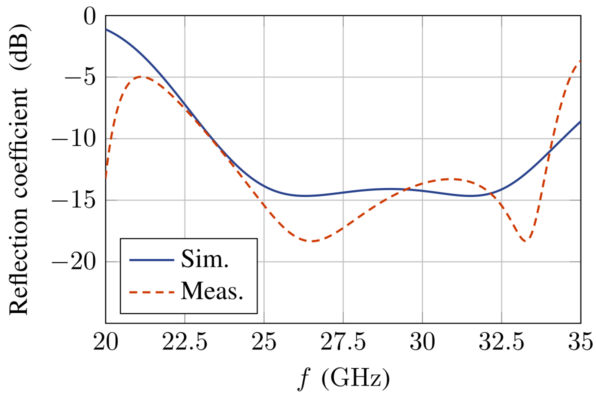

(a)

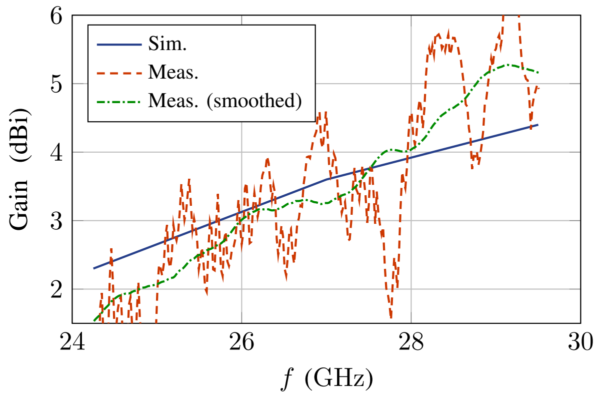

(b)

Fig. 6: Measured and simulated a) active reflection coefficient and b) gain of the proposed magneto-electric dipole antenna.

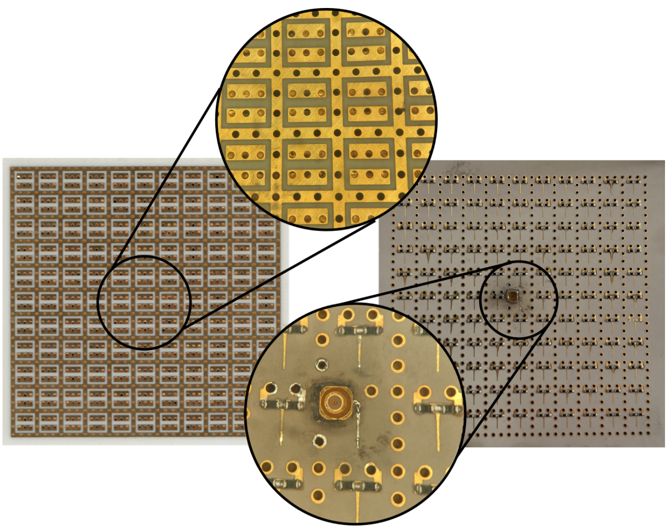

Fig. 5: Top (left) and bottom (right) view of the 11 × 11 prototype of the proposed magneto-electric dipole antenna.

array prototype is used, the array performance is verified through an embedded element pattern measurement. This reduces the hardware complexity and thus providing a cost-efficient characterization technique [10]. For this purpose, only the center element of the array is fed while all others are terminated with two $100\,\Omega$ resistors in parallel (see Fig. 5). For the feeding, an SMPS PCB connector with a small diameter of $2.54\,\mathrm{mm}$ from SV Microwave was used enabling an easy integration within the center UC. The simulated active reflection coefficient of the infinite array simulation and the measured reflection coefficient of the embedded element are depicted in Fig. 6a. The measurement results demonstrate good agreement with the infinite array simulation, with the measured reflection coefficient being below $-10\,\mathrm{dB}$ for a frequency range from $23.3\,\mathrm{GHz}$ to $34.1\,\mathrm{GHz}$. A comparison of the simulated and measured antenna gain is given in Fig. 6b. The measured antenna gain exhibits ripples arising from an coaxial to SMPS adapter. In the antenna gain measurement, only the transmission losses of the adapter are compensated. However, the smoothed measured gain aligns well with the simulation results within the desired frequency band (see Fig. 6b).

The simulation and measurement results of the embedded element pattern in the co- and cross-polarization are depicted in Fig. 7 for the E-plane and in Fig. 8 for the H-plane, respectively. In order to verify the radiation performance across the desired frequency band, a comparison is taken at the lower

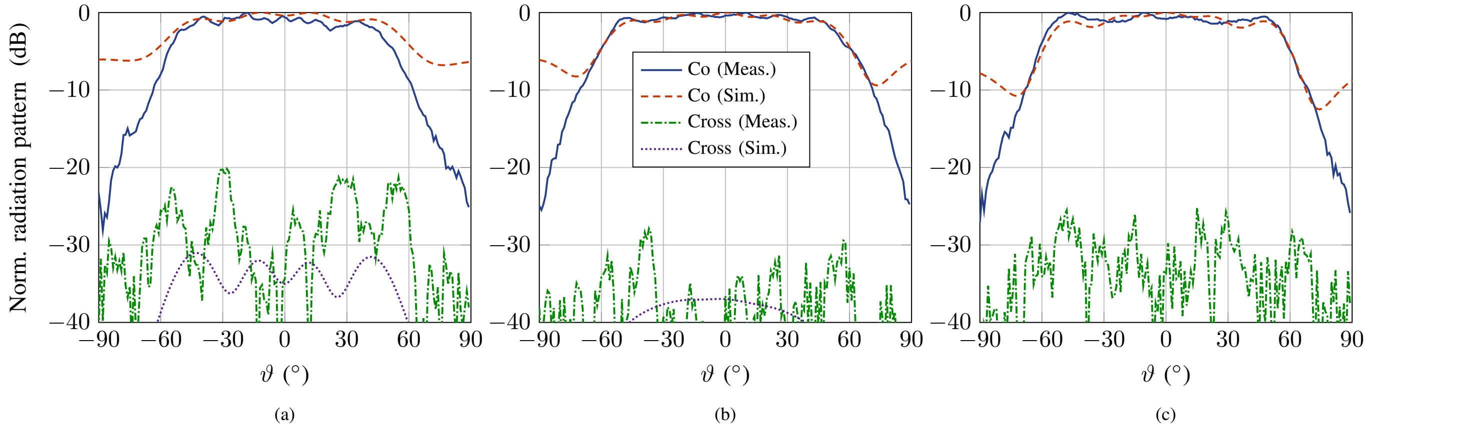

Fig. 7: Measured and simulated embedded element pattern of the proposed magneto-electric dipole antenna at a) 24.25 GHz, b) 27 GHz, and c) 29.5 GHz in the E-plane.

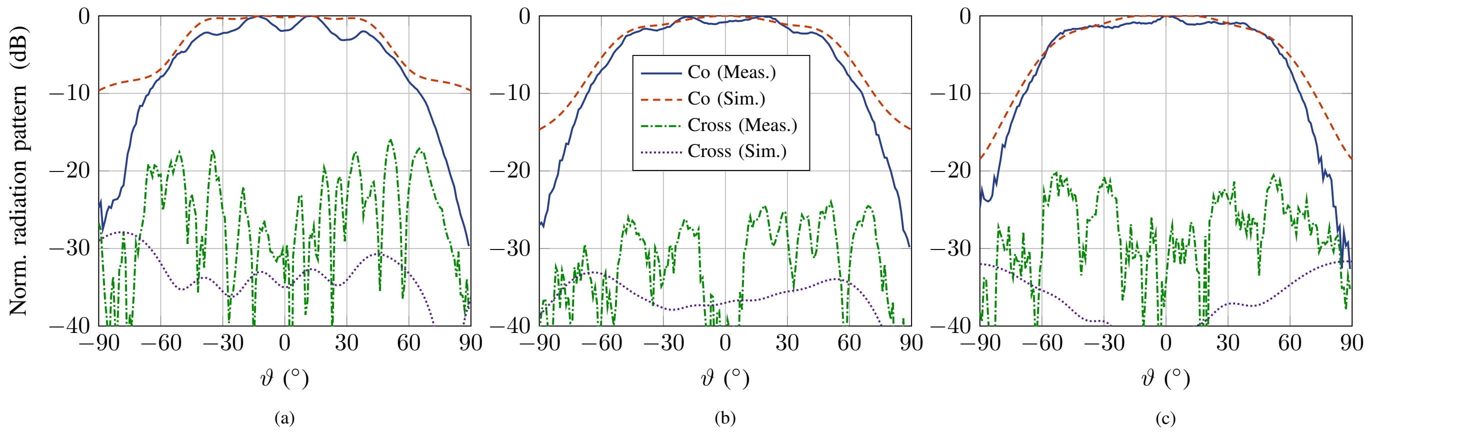

Fig. 8: Measured and simulated embedded element pattern of the proposed magneto-electric dipole antenna at a) 24.25 GHz, b) 27 GHz, and c) 29.5 GHz in the H-plane.

and upper ends of the frequency band, as well as for the center frequency. The measured patterns show an excellent agreement with the simulation results. In both, the E- and H-plane ripples can be observed in the simulation and measured embedded element pattern, resulting from the parasitic radiation at the edges of the finite 11×11 prototype antenna. For larger arrays this phenomenon can be neglected. The measured cross-polarization level in the E- and H-plane is lower than -15 dB. In both, the E- and H-plane the measured cross-polarization level appears to be higher than expected from the simulation results. This can be explained by manufacturing and assembly tolerances.

V. Conclusion

In this paper, a novel unit cell design of a low-profile magneto-electric dipole antenna is presented. The antenna operates from 24.25 GHz to 29.5 GHz, covering multiple frequency bands for the 5G communication networks. An infinite array analysis was conducted to evaluate and optimize the antenna design for wide-scanning performance, achieving up to 60° in the E- and 30° in the H-plane, respectively. Subsequently, a 11×11 prototype antenna has been manufactured and characterized, verifying the simulation results. The reflection coefficient of the embedded element remains below -10 dB from 23.3 GHz to 34.1 GHz, demonstrating good agreement with the simulation results of the infinite array. Additionally, the simulated and measured antenna gain coincide well in the operational frequency band from 24.25 GHz to 29.5 GHz. The measured embedded element patterns show excellent agreement with the simulation results.

Acknowledgment

This work was supported by the German Research Foundation (DFG) under Grant CH 2226/2-1.

References

[1] M. Fischer, C. Waldschmidt, and T. Chaloun, "Wide-angle scanning coupled dipole antenna array for heterogeneous mm-wave communication networks," in *2023 17th European Conference on Antennas and Propagation (EuCAP)*, 2023, pp. 1–5.

[2] T. Chaloun, L. Boccia, E. Arnieri, M. Fischer, V. Valenta, N. J. G. Fonseca, and C. Waldschmidt, "Electronically steerable antennas for future heterogeneous communication networks: Review and perspectives," *IEEE Journal of Microwaves*, vol. 2, no. 4, pp. 545–581, 2022.

[3] S. M. Moghaddam, A. Uz Zaman, J. Yang, and A. A. Glazunov, "Ultrawide band tightly-coupled aperture magneto-electric dipole array over 20 - 40 ghz," in *2019 13th European Conference on Antennas and Propagation (EuCAP)*, 2019, pp. 1–3.
[4] J. Sun, A. Li, and K.-M. Luk, "A high-gain millimeter-wave magneto-electric dipole array with packaged microstrip line feed network," *IEEE Antennas and Wireless Propagation Letters*, vol. 19, no. 10, pp. 1669–1673, 2020.
[5] M. Li and K.-M. Luk, "Wideband magneto-electric dipole antenna for 60-ghz millimeter-wave communications," *IEEE Transactions on Antennas and Propagation*, vol. 63, no. 7, pp. 3276–3279, 2015.
[6] S. Targonski, R. Waterhouse, and D. Pozar, "Design of wide-band aperture-stacked patch microstrip antennas," *IEEE Transactions on Antennas and Propagation*, vol. 46, no. 9, pp. 1245–1251, 1998.
[7] C. Vasanelli, T. Ruess, and C. Waldschmidt, "A 77-ghz cavity antenna array in pcb technology," in *2015 IEEE 15th Mediterranean Microwave Symposium (MMS)*, 2015, pp. 1–4.
[8] *HFSS Version 19.2*, Ansys Cooperation, Canonsburg, PA, USA, 2019.
[9] G. Knittel, A. Hessel, and A. Oliner, "Element pattern nulls in phased arrays and their relation to guided waves," *Proceedings of the IEEE*, vol. 56, no. 11, pp. 1822–1836, 1968.
[10] D. Pozar, "The active element pattern," *IEEE Transactions on Antennas and Propagation*, vol. 42, no. 8, pp. 1176–1178, 1994.